Arch. Metall. Mater. **66** (2021), 4, 1105-1113

DOI: 10.24425/amm.2021.136430

A. TAJDEEN[1], A. MEGALINGAM[1*]

OPTIMIZATION OF OUTPUT RESPONSES DURING EDM OF AZ91 MAGNESIUM ALLOY USING GREY RELATIONAL ANALYSIS AND TOPSIS

Unconventional machining of magnesium alloys through die sinking and Wire Electrical Discharge Machining (WEDM) processes are preferred over conventional machining processes to overcome the rapid loss in strength and affinity that occurs with tool materials at high temperatures. In the present study, AZ91 magnesium alloy is machined in EDM using a prepared alloy tool (copper alloyed with titanium diboride). Based on Taguchi's L_{27} orthogonal array, a total of 27 experiments have been conducted by varying the process parameters such as pulse on time (T_{on}), gap voltage (V_g) and current (I_p) with three different levels. Techniques for Order Preference by Similarity to Ideal Solution (TOPSIS) and Grey Relational Analysis (GRA) have been applied to optimize the response parameters of EDM to obtain maximum Material Removal rate (MRR) and minimum Tool Wear Rate (TWR) and Surface Roughness (SR). Analysis of variance (ANOVA) is carried out based on F-test at a confidence interval of 95% to confirm the significant influence of individual parameters. From the above two optimization techniques, the obtained optimal values are current 15 A, gap voltage 55 V, pulse on time 30 µs and an error of less than 5% is observed from the confirmation experiments. Scanning Electron microscope (SEM) images revealed that there is no formation of cracks but micro pits and holes are observed.

Keywords: AZ91 Magnesium Alloy, EDM, TOPSIS, GRA, and ANOVA

1. Introduction

In the last two decades, magnesium and its alloys are the most attractive engineering materials in automobile, aerospace, biomedical and defense applications due to its low density of 1.74 g/cm^3, good weight to strength ratio, high energy absorption characteristics and good specific stiffness [1-4]. Aluminium and zinc-based magnesium alloys are the best choices for many applications because of 22% to 70% of weight reduction. The AZ91 magnesium alloy has 9% of aluminum, 1% of zinc and the rest is magnesium. In addition to that soluble and semi-soluble elements increased the mechanical, machining, wear, and fatigue properties of the materials [5]. Magnesium and its alloys show the rapid loss in strength and affinity with tool materials at a high temperature which leads to reduced usage of conventional machining processes in structural applications. EDM is one of the best preferred electrical energy-based unconventional material removal processes for mold making, die making, automotive, aerospace, and surgical components fabrications. It also allows machining the components having complex contours and to attain good surface texture [6,7]. EDM is feasible to apply all electrical conducting materials irrespective of their mechanical properties. By proper selection of input parameters in the EDM process yields better performance characteristics such as increased material removal rate, decreased tool wear rate and better surface roughness [8,9]. The effect of SiC addition in pure magnesium through powder metallurgy technique was investigated through EDM by changing the input parameters such as pulse on time, current and pulse off time. Results revealed that the material removal rate increases as the current increases. The high tool wear rate was observed for increased pulse off-time but it is reversed for the pulse on time [10]. The addition of rare earth elements in magnesium increased the corrosion resistance and creep strength. EDM response characteristics were optimized using the multi-objective passing vehicle search algorithm. The theoretically calculated MRR, TWR, and roundness of holes with help of a computational model developed using Response Surface Methodology (RSM) leads to a reduced number of experimental trials [11]. Aluminum and graphite nano-powders mixed dielectric fluid in the EDM process of magnesium alloys helps to improve the MRR due to effective discharge breakdown between the tool and workpiece. The results show that the most influencing parameters are pulse on time and current [12,13]. Brass, copper, aluminum, tungsten mixed with copper,

[1] BANNARI AMMAN INSTITUTE OF TECHNOLOGY, DEPARTMENT OF MECHANICAL ENGINEERING, SATHYAMANGALAM, ERODE-638401, TAMIL NADU, INDIA

* Corresponding author: mechmega@gmail.com

and GRAL-20 (composite tool) were taken as tool materials for machining AZ91/5B_4C_p material matrix composite in the EDM process. The surface finish of AZ91/5B_4C_p is good when machining with GRAL-20 tool material as the re-melted layer and black spots on the workpiece is eliminated [14]. In recent research works, different machining processes are utilized in various optimization techniques such as GRA [15,16], TOPSIS [17,18], RSM [18], Non-Dominated Sorting Genetic Algorithm (NSGA) [19] and Multi-Objective Optimization by Ratio Analysis (MOORA) [20] to convert multi-response into a single response in order to analyze the impact of input parameters on the output responses.

From the literature survey, it is evident that only a few research works were focused on machining of magnesium and its alloys using EDM. As a consequence of that, most of the researchers have concentrated on machining performance characteristics of MRR and TWR using copper tool material. In the present work, a special attempt is made on the EDM process of AZ91 magnesium alloy using copper mixed titanium diboride as a tool material. The GRA and TOPSIS techniques are used to obtain the optimal EDM machining parameters for high MRR with low TWR and SR. The ANOVA is carried out to identify the best significant EDM process parameters. The scanning electron microscope images are taken for the optimal condition to explore the microstructural characteristics.

2. Materials and experimental procedure

In this investigation, AZ91 magnesium alloy is selected as work material. The elemental composition of the work material is given in Table 1. The samples are cut into a dimension of 100×25×5 mm. It is observed that, the powder metallurgy technique based tool electrode provides no micro-cracks, high micro hardness in the machined surface and high MRR with low TWR [21,22], In this way, the current tool is prepared with equal amount of titanium diboride and copper powders having average particle size of 44 µm, are taken and blended in a ball milling for 10 hours. The mixer is then compacted and sintered to fabricate the tool with a load of 14 Ton. The experimentally calculated density of the tool is 6.743 g/cm^3. Further, the tool is brazed with copper in order to mount in the EDM machine. The prepared 15 mm Copper alloyed with titanium diboride (Cu-TiB_2) tool is shown in Fig. 1a. The CNC-based EDM machine as shown in Fig. 1b is used to carry out the experiments with EDM oil as dielectric fluid. The tool is connected with a cathode power supply and the worktable is connected with an anode power supply. The EDM oil is flushed at a pressure of 0.5 MPa during the machining and maintained at a constant pulse off time of 15 µs.

The operating conditions of EDM process are controlled by the various input process parameters. Based on literature survey [13,23] and from pilot study experiments, the present input parameters such as current (I_p), gap voltage (V_g) and pulse on time (T_{on}) and their levels are selected which is listed in Table 2. Design of experiments is the systematic procedural method to carry out experiments in proper order or sequence to establish the correlation among the factors considered for this study. Based on Taguchi's L_{27} orthogonal array, experiments are conducted and response parameters such as MRR, TWR and SR values are obtained which are listed in Table 3. Three trials are conducted for each experimental run.

TABLE 1

Elemental composition of Work material

Element	Al	Zn	Mn	Si	Ni	Fe	Cu	Mg
Weight Percentage (%)	9.1	0.68	0.21	0.085	0.0021	0.001	0.001	Balance

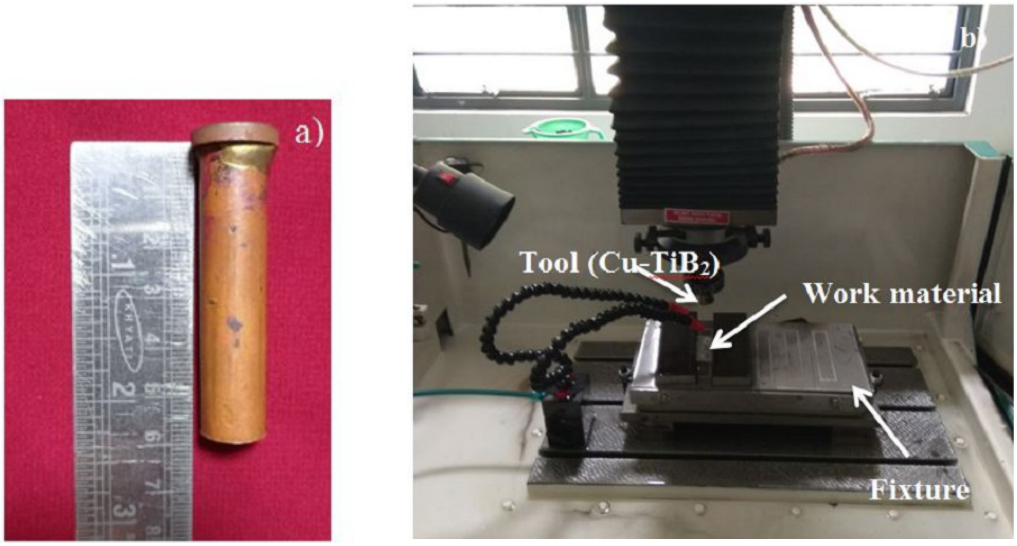

Fig. 1. a) Tool, b) Die sink EDM machine

TABLE 2

Levels of various Input process parameters

Factors	Levels		
	I	II	III
Current I_p, (A)	5	10	15
Gap Voltage V_g, (V)	50	55	60
Pulse on Time T_{on}, (µs)	10	20	30

3. Result and discussions

3.1. Mechanism of Material Removal Rate (MRR)

Generally, the efficiency of the EDM process is described by MRR and TWR. In the EDM process, the predominant material removal takes place due to diffusion between electrodes. In order to increase the machining rate, the materials having high electrical conductivity and melting point are selected as tool materials. The main inevitable objective of the machining process is to increase the MRR and decrease the TWR. The variation in MRR with respect to current and pulse on time is shown in Fig. 2a. A gradual increase in material removal rate is occurred due to the increase in current and pulse on time as the particles from the tool get removed and drifts inside the spark gap. Fig. 2b shows the variation of MRR against voltage and pulse on time. When the pulse on time increases the discharge energy is also increases which results in high metal erosion and vaporization at the samples due to short circuits, bridging effect and earlier explosion [24]. Fig. 2c shows the variation of MRR against voltage and current. Initially, when there is an increase in voltage and current leads to more discharge power which results in melting of the samples. When the voltage crosses 56 volts, the instability and frequency of short circuits increase, as a result, the plasma channel gets widened and enlarged.

TABLE 3

L_{27} experimental design with response parameters values

Exp no.	Input process parameters			Response parameters		
	Current (I_p)	Gap Voltage (V_g)	Pulse on time (T_{on})	Avg MRR	Avg TWR	Avg SR
	A	V	µs	g/min	g/min	µm
1.	5	50	10	0.0180	0.0006362	1.7183
2.	5	50	20	0.0440	0.0012300	1.4137
3.	5	50	30	0.0740	0.0016520	1.5927
4.	5	55	10	0.0230	0.0008724	1.6203
5.	5	55	20	0.0450	0.0004166	1.7883
6.	5	55	30	0.0630	0.0005263	1.6120
7.	5	60	10	0.0226	0.0002220	1.8510
8.	5	60	20	0.0479	0.0004319	1.5687
9.	5	60	30	0.0717	0.0005880	1.5360
10.	10	50	10	0.0278	0.0024570	1.7097
11.	10	50	20	0.0580	0.0004878	1.7260
12.	10	50	30	0.1260	0.0014850	1.5147
13.	10	55	10	0.0262	0.0022600	1.6507
14.	10	55	20	0.0630	0.0007633	1.8637
15.	10	55	30	0.1219	0.0062820	1.4017
16.	10	60	10	0.0278	0.0016290	1.4877
17.	10	60	20	0.0720	0.0006194	1.8107
18.	10	60	30	0.1300	0.0041020	1.3047
19.	15	50	10	0.0330	0.0058460	1.4127
20.	15	50	20	0.0645	0.0022850	1.1993
21.	15	50	30	0.1446	0.0047530	1.4243
22.	15	55	10	0.0316	0.0053230	1.5993
23.	15	55	20	0.0732	0.0032250	1.5877
24.	15	55	30	0.1790	0.0072830	1.1033
25.	15	60	10	0.0331	0.0045900	1.3977
26.	15	60	20	0.0725	0.0037500	1.5327
27.	15	60	30	0.1540	0.0061340	1.1267

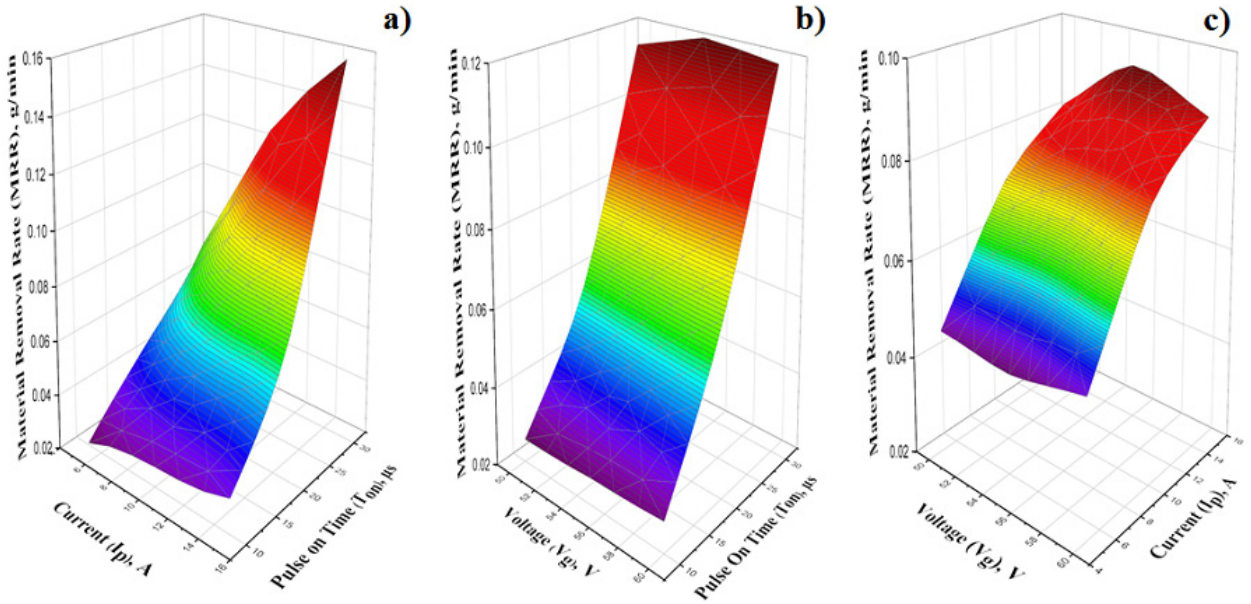

Fig. 2. 3D plots of a) MRR vs Current &Pulse on time b) MRR vs Voltage & Pulse on time c) MRR vs Current & Voltage

3.2. Mechanism of Tool Wear Rate (TWR)

Fig. 3a shows the variation of TWR against current and pulse on time. An increase in pulse duration reduces the TWR up to 0.0013 g/min till T_{on} of 20 µs due to a decrease in temperature which is less than the melting point of the tool. Beyond the T_{on} of 20 µs, the TWR starts to increase as the plating build-up is started and no voltage excitation from the tool is evident which is also observed in M. Ghoreishi et al. [25]. A small amount of decrease in TWR is observed due to an increase in current. Fig. 3b shows the variation of TWR against voltage and pulse on time. Prolonged pulse on time increases the energy density which leads to increase in tool wear rate [26]. Fig. 3c shows the variation of TWR against the current and voltage. TWR is increased due to peak current and its corresponding voltage results in high discharge current flows in the tool which leads to plasma channel formation. Spark energy depends on applied voltage and field strength of electricity, is increased up to a certain level and higher voltage setting in the gap which changes the flushing state.

3.3. Surface Roughness (SR)

Fig. 4a-c shows the variation of surface roughness against the current, voltage, and pulse on time. The EDM is not only affects the surface it also affects the sub-surfaces (secondary layers). The size and type of the crater developed during machining and scattering of the improved layer (Recast layer) directly relate to the surface quality of the machined component. The low

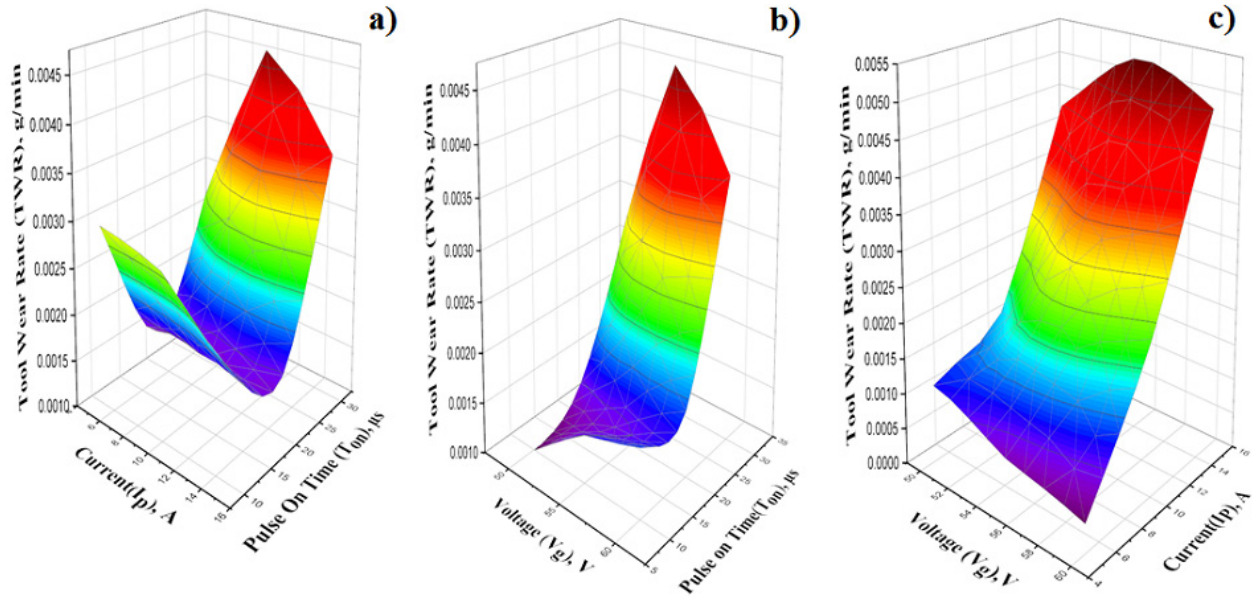

Fig. 3. 3D plots of a) TWR vs Current & Pulse on time b) vs Voltage & Pulse on time c) TWR vs Current & Voltage

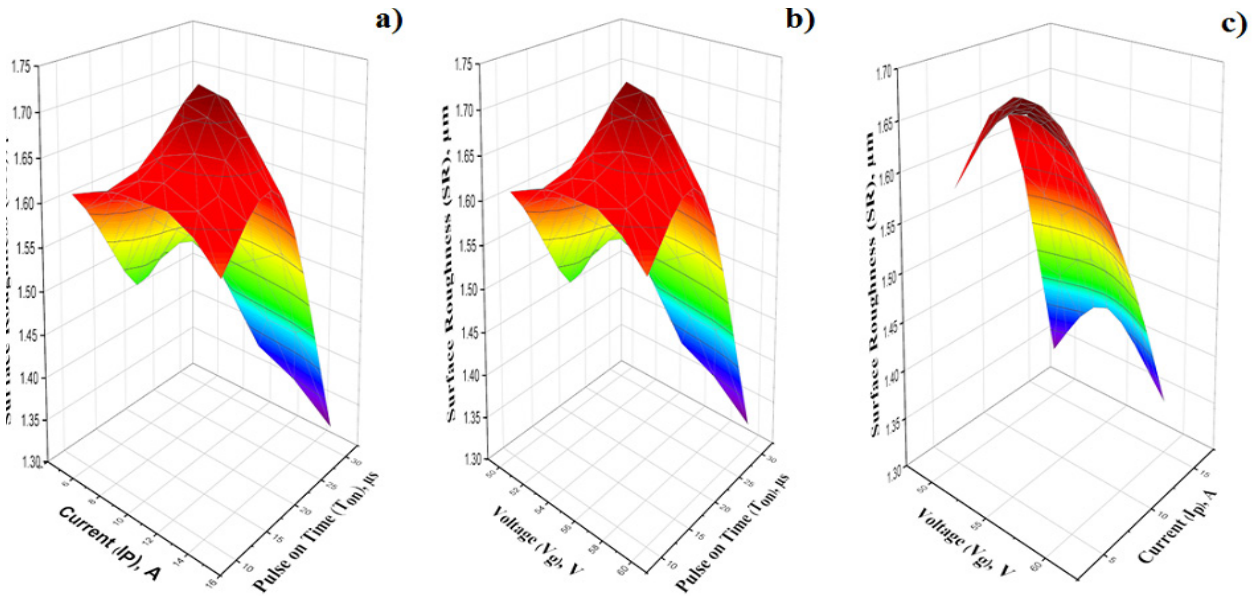

Fig. 4. 3D plots of a) SR vs Current &Pulse on time b) SR vs Voltage & Pulse on time c) SR vs Current & Voltage

voltage, low current, and minimum pulse on time condition have produced a low concentrated plasma channel which causes more roughness on the machined surface because of the formation of the more liquid crater with a small-diameter [27]. When there is an increase in pulse on time a strong plasma channel develops which decreases the surface roughness due to low spark intensity at the discharge spot [14].

3.4. GRA – Technique for Multi-response optimization

The optimum parameters setting for multi-responses of EDM was achieved through multi-response optimization techniques. One of the best preferred multi-response optimization techniques is GRA and used to find the finest solution among all possible combinations of multiple performance characteristics [15,28,29].

In GRA, the first step is experimental values are normalized. The normalized values range within zero to one and those values named as "Grey Relational Generation (GRG)". Taguchi's higher the better principle was used to calculate GRG of MRR. The formula of GRG for MRR is given as

$$C_i^*(k) = \frac{y_i(l) - \min y_i(l)}{\max y_i(l) - \min y_i(l)} \tag{1}$$

For GRG of TWR and Surface Roughness corresponding to lower the better principle is given as

$$C_i^*(k) = \frac{\max y_i - y_i(l)}{\max y_i(l) - \min y_i(l)} \tag{2}$$

Where $C_i^*(k)$ found after the "GRG". The next step is formulating the relationship between normalized and finest values with help of the calculated Grey Relational Coefficient (GRC). The GRC is calculated using the expression as

$$\gamma(x_o(l), x_i(l)) = \frac{\Delta\min + \zeta\Delta\max}{\Delta_{oi}(l) + \zeta\Delta\max} \tag{3}$$

Where $\Delta_{oi}(l) = |x_0(l) - x_1(l)|$. $x_0(l)$ is the reference sequnce, ζ is distinctive coefficient lying between 0 to 1. Δmin, Δmax are minimum and maximum values for Δ_{oi} respectively. The final step is the calculation of GRG value from GRC values for each experimental run.

$$\gamma(x_o, x_i) = \frac{1}{m}\sum_{i=1}^{m}\gamma(x_o(k), x_i(k)), \quad k \text{ to } 1 \tag{4}$$

The highest value of grey relational grades indicates the value nearer to the optimum solution.

The output obtained from experiments is tabulated in Table 4. The obtained results are normalized using Eq. (1) and Eq. (2). GRC and GRG for each response are calculated using

TABLE 4

Normalized, GRC, GRG values and Rank of Experimental results

Exp. no	Measured values			Normalized			GRC			GRG	Rank
	Avg MRR	Avg TWR	Avg SR	Avg MRR	Avg TWR	Avg SR	Avg MRR	Avg TWR	Avg SR		
1.	0.018	0.00063	1.718	0.0000	0.9362	0.1912	0.3333	0.8868	0.3820	0.5341	16
2.	0.044	0.00123	1.414	0.1615	0.8525	0.5919	0.3735	0.7722	0.5506	0.5655	10
3.	0.074	0.00165	1.593	0.3478	0.7931	0.3565	0.4340	0.7073	0.4372	0.5262	18
4.	0.023	0.00087	1.620	0.0311	0.9029	0.3201	0.3404	0.8374	0.4238	0.5338	17
5.	0.045	0.00042	1.788	0.1677	0.9671	0.0991	0.3753	0.9383	0.3569	0.5568	12
6.	0.063	0.00053	1.612	0.2795	0.9516	0.3311	0.4097	0.9118	0.4277	0.5831	8
7.	0.023	0.00022	1.851	0.0286	0.9945	0.0167	0.3398	0.9891	0.3371	0.5553	14
8.	0.048	0.00043	1.569	0.1857	0.9649	0.3880	0.3804	0.9345	0.4497	0.5882	6
9.	0.072	0.00059	1.536	0.3335	0.9430	0.4310	0.4286	0.8976	0.4677	0.5980	5
10.	0.028	0.00246	1.710	0.0609	0.6797	0.2026	0.3474	0.6095	0.3854	0.4475	25
11.	0.058	0.00049	1.726	0.2484	0.9571	0.1811	0.3995	0.9209	0.3791	0.5665	9
12.	0.126	0.00149	1.515	0.6708	0.8166	0.4591	0.6030	0.7317	0.4803	0.6050	4
13.	0.026	0.00227	1.651	0.0509	0.7075	0.2802	0.3450	0.6309	0.4099	0.4619	23
14.	0.063	0.00076	1.864	0.2795	0.9183	0.0000	0.4097	0.8595	0.3333	0.5342	15
15.	0.122	0.00628	1.402	0.6453	0.1410	0.6077	0.5850	0.3679	0.5603	0.5044	20
16.	0.028	0.00163	1.488	0.0609	0.7963	0.4946	0.3474	0.7106	0.4973	0.5184	19
17.	0.072	0.00062	1.811	0.3354	0.9385	0.0698	0.4293	0.8905	0.3496	0.5565	13
18.	0.130	0.00410	1.305	0.6957	0.4480	0.7353	0.6216	0.4753	0.6538	0.5836	7
19.	0.033	0.00585	1.413	0.0932	0.2024	0.5932	0.3554	0.3853	0.5514	0.4307	26
20.	0.065	0.00229	1.199	0.2888	0.7039	0.8738	0.4128	0.6281	0.7985	0.6131	3
21.	0.145	0.00475	1.424	0.7863	0.3563	0.5779	0.7006	0.4372	0.5422	0.5600	11
22.	0.032	0.00532	1.599	0.0845	0.2761	0.3477	0.3532	0.4085	0.4339	0.3986	27
23.	0.073	0.00323	1.588	0.3430	0.5715	0.3631	0.4321	0.5385	0.4398	0.4702	21
24.	0.179	0.00728	1.103	1.0000	0.0000	1.0001	1.0000	0.3333	1.0000	0.7778	1
25.	0.033	0.00459	1.398	0.0938	0.3793	0.6130	0.3556	0.4461	0.5637	0.4551	24
26.	0.073	0.00375	1.533	0.3385	0.4976	0.4354	0.4305	0.4988	0.4697	0.4663	22
27.	0.154	0.00613	1.127	0.8447	0.1618	0.9694	0.7630	0.3736	0.9423	0.6930	2

Eq. (3) and Eq. (4) is given in Table 4. The overall effect of the process attributes on machining is assessed using GRG values. The experimental run 24 yields the optimal result because of the higher GRG value among all 27 experiments.

3.4.1. ANOVA for GRA

To obtain the most significant parameters which affect the response parameters of EDM is found using Analysis of variance (ANOVA). The ANOVA is constructed by using GRG values with help of MINITAB software and it is tabulated in Table 5. The ANOVA table reveals that the most significant parameter is the pulse on time with P value 0.002 and the rank of input parameters as listed in Table 6.

TABLE 5

ANOVA for grey relational grade

Source of Variation	DF	Seq SS	Adj SS	Adj MS	F	P
I_p	2	0.003989	0.003989	0.001995	0.67	0.529
V_g	2	0.002438	0.002438	0.001219	0.41	0.673
T_{on}	2	0.066769	0.066769	0.033384	11.23	0.002
$(V_g) \times (T_{on})$	4	0.014272	0.014272	0.003568	1.20	0.360
$(I_p) \times (T_{on})$	4	0.044104	0.044104	0.011026	3.71	0.035
Error	12	0.035681	0.035681	0.002973		
Total	26	0.167253				

TABLE 6

Response table for grey relational grade

Level	I_p	V_g	T_{on}
1	0.5601	0.5387	0.4817
2	0.5309	0.5356	0.5464
3	0.5405	0.5572	0.6034
Delta	0.0292	0.0215	0.1217
Rank	2	3	1

3.5. TOPSIS

TOPSIS is a conceptual-based simple ranking method for complex problem-solving in decision-making areas of manufacturing. The performance of the machining process is influenced by a number of measures, alternatives and their relationship [17,28,29]. For the study of response attributes MRR should be larger the better and TWR, SR should be smaller the better.

Step 1: Construct the decision matrix with z attributes and x alternatives to represent the result of the experiments with various response parameters.

$$M_D = \begin{bmatrix} y_{11} & y_{12} & \cdots & \cdots & \cdots & y_{1z} \\ y_{21} & y_{22} & \cdots & \cdots & \cdots & y_{2z} \\ y_{31} & y_{32} & \cdots & \cdots & \cdots & y_{3z} \\ \vdots & \vdots & \vdots & \ddots & \ddots & \vdots \\ \vdots & \vdots & \vdots & \ddots & \ddots & \vdots \\ y_{x1} & y_{x2} & \cdots & \cdots & \cdots & y_{xz} \end{bmatrix}$$

Where y_{ij} is the response variable of the i^{th} row in relation to the j^{th} column.

Step 2: Normalized matrix calculation using Eq. (5)

$$M_n = \frac{y_{ij}}{\sqrt{\sum_{i=1}^{x} y_{ij}^{\,2}}}, \quad \text{here } j = 1,2,\ldots,z \tag{5}$$

Step 3: The weighted normalized decision matrix and relative importance of attributes are calculated using entropy analysis Eq. (6)

$$C = M_n V_j, \ \text{where} \ \sum_{j=1}^{z} V_j = 1 \tag{6}$$

Step 4: Find the positive and negative ideal solutions from Eq. (7) and Eq. (8)

$$k^{+} = \left\{ \begin{pmatrix} \max \\ \sum_i c_{ij} \mid j \in L \end{pmatrix}, \\ \begin{pmatrix} \min \\ \sum_i \mid j \int L \mid i = 1,2....,x \end{pmatrix} \right\} = c_1^{+}, c_2^{+}, c_3^{+}, ...c_n^{+}\} \tag{7}$$

$$k^{-} = \left\{ \begin{pmatrix} \min \\ \sum_i c_{ij} \mid j \in L \end{pmatrix}, \\ \begin{pmatrix} \max \\ \sum_i \mid j \int L \mid i = 1,2....,x \end{pmatrix} \right\} = c_1^{-}, c_2^{-}, c_3^{-}, ..., c_n^{-}\} \tag{8}$$

The separation between the alternatives was calculated using Eq. (9) and Eq. (10).

For a positive ideal solution

$$F_1^{+} = \sqrt{\sum_{j=i}^{z} \left(c_{ij} - c_j^{+}\right)^2}, \quad i = 1,2,....,x \tag{9}$$

For the negative ideal solution

$$F_1^{-} = \sqrt{\sum_{j=i}^{z} \left(c_{ij} - c_j^{-}\right)^2}, \quad i = 1,2,....,x \tag{10}$$

Step 5: For each alternative, calculate the closeness coefficient with respect to the ideal solution using Eq. (11)

$$q_i = \frac{F_i^{-}}{F_i^{+} + F_i^{-}}, \quad i = 1,2,....,x \tag{11}$$

Step 6: Finally rank the alternatives in descending order to find the most and least favored solutions.

Taguchi's design is combined with TOPSIS is used to find closeness coefficient to the ideal solution for each experimental run is listed in Table 7. From Table 7, the experimental run 24 gives the optimal result because of the maximum closeness coefficient to the ideal solution among all 27 experiments.

3.5.1. ANOVA for TOPSIS

The ANOVA is constructed by using closeness coefficient with help of MINITAB software and it is listed in Table 8. The ANOVA reveals that pulse on time and current are the most

TABLE 7

Normalized, weighted normalized, closeness coefficient and Rank of Experimental results

Exp. No	Measured values			Normalized			Weighted normalized			Closeness coefficient	Rank order
	Avg MRR	Avg TWR	Avg SR	Avg MRR	Avg TWR	Avg SR	Avg MRR	Avg TWR	Avg SR		
1.	0.018	0.00063	1.718	0.0426	0.0364	0.2131	0.0220	0.0068	0.0629	0.2668	21
2.	0.044	0.00123	1.414	0.1042	0.0703	0.1753	0.0538	0.0132	0.0518	0.3088	18
3.	0.074	0.00165	1.593	0.1752	0.0944	0.1975	0.0905	0.0178	0.0583	0.4148	9
4.	0.023	0.00087	1.620	0.0545	0.0499	0.2009	0.0281	0.0094	0.0593	0.2675	20
5.	0.045	0.00042	1.788	0.1066	0.0238	0.2217	0.0550	0.0045	0.0655	0.3306	17
6.	0.063	0.00053	1.612	0.1492	0.0301	0.1999	0.0771	0.0057	0.0590	0.3918	10
7.	0.023	0.00022	1.851	0.0535	0.0127	0.2295	0.0276	0.0024	0.0678	0.2848	19
8.	0.048	0.00043	1.569	0.1134	0.0247	0.1945	0.0586	0.0046	0.0574	0.3405	16
9.	0.072	0.00059	1.536	0.1698	0.0336	0.1905	0.0877	0.0063	0.0563	0.4269	7
10.	0.028	0.00246	1.710	0.0658	0.1404	0.2120	0.0340	0.0264	0.0626	0.2231	24
11.	0.058	0.00049	1.726	0.1373	0.0279	0.2140	0.0709	0.0052	0.0632	0.3730	13
12.	0.126	0.00149	1.515	0.2984	0.0849	0.1878	0.1541	0.0160	0.0555	0.6849	4
13.	0.026	0.00227	1.651	0.0620	0.1291	0.2047	0.0320	0.0243	0.0605	0.2276	23
14.	0.063	0.00076	1.864	0.1492	0.0436	0.2311	0.0771	0.0082	0.0683	0.3857	11
15.	0.122	0.00628	1.402	0.2887	0.3590	0.1738	0.1491	0.0676	0.0513	0.5701	6
16.	0.028	0.00163	1.488	0.0658	0.0931	0.1845	0.0340	0.0175	0.0545	0.2544	22
17.	0.072	0.00062	1.811	0.1705	0.0354	0.2245	0.0881	0.0067	0.0663	0.4267	8
18.	0.130	0.00410	1.305	0.3078	0.2344	0.1618	0.1590	0.0441	0.0478	0.6529	5
19.	0.033	0.00585	1.413	0.0781	0.3341	0.1752	0.0404	0.0629	0.0517	0.1334	26
20.	0.065	0.00229	1.199	0.1527	0.1306	0.1487	0.0789	0.0246	0.0439	0.3629	15
21.	0.145	0.00475	1.424	0.3424	0.2716	0.1766	0.1769	0.0511	0.0522	0.7043	2
22.	0.032	0.00532	1.599	0.0748	0.3042	0.1983	0.0387	0.0573	0.0586	0.1314	27
23.	0.073	0.00323	1.588	0.1734	0.1843	0.1969	0.0896	0.0347	0.0581	0.3774	12
24.	0.179	0.00728	1.103	0.4239	0.4162	0.1368	0.2189	0.0783	0.0404	0.7109	1
25.	0.033	0.00459	1.398	0.0784	0.2623	0.1733	0.0405	0.0494	0.0512	0.1715	25
26.	0.073	0.00375	1.533	0.1717	0.2143	0.1900	0.0887	0.0403	0.0561	0.3632	14
27.	0.154	0.00613	1.127	0.3647	0.3505	0.1397	0.1884	0.0660	0.0413	0.6910	3

significant parameters with P value 0.000 for the both significant parameters and the rank of input parameters as listed in Table 9.

TABLE 8

ANOVA for closeness coefficient

Source of Variation	DF	Seq SS	Adj SS	Adj MS	F	P
I_p	2	0.036530	0.036530	0.018265	36.96	0.000
V_g	2	0.002733	0.002733	0.001366	2.77	0.103
T_{on}	2	0.608671	0.608671	0.304335	615.81	0.000
$(V_g) \times (T_{on})$	4	0.135857	0.135857	0.033964	68.73	0.360
$(I_p) \times (T_{on})$	4	0.003240	0.003240	0.000810	1.64	0.035
Error	12	0.005930	0.005930	0.000494		
Total	26	0.792962				

TABLE 9

Response table for closeness coefficient

Level	I_p	V_g	T_{on}
1	0.3369	0.3858	0.2178
2	0.4220	0.3770	0.3632
3	0.4051	0.4013	0.5831
Delta	0.0851	0.0243	0.3653
Rank	2	3	1

3.6. Comparison of GRA and TOPSIS

The GRG values in GRA and closeness coefficient of the TOPSIS are found to be nearly equal for the experimental trials as shown in Fig. 5. The optimum process parameters obtained from GRA and TOPSIS techniques revealed the same result with a 95% confidence interval. Confirmation experiments are conducted and found that predicted and calculated values for the output responses of MRR, TWR and SR are obtained less than 3% error. It determines that error values lie within the satisfactory level of less than 5%.

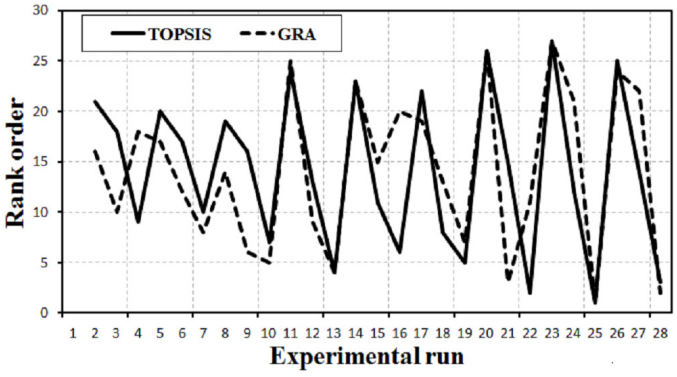

Fig. 5. Comparison of GRA and TOPSIS

3.7. Microstructure analysis

Fig. 6a and 6b show the SEM images of optimal machining condition. In Fig. 6a, there are no cracks were found but micro pits and holes are observed. From Fig. 6b, it is observed that the uniform melting and proper flushing lead to minimum re-heated layers which results in better surface quality compared to other operating conditions.

The micrographs for the Current 15 A, voltage 55 V and Pulse on Time 30 µs machining condition are shown in Fig. 7a and 7b, at this condition, deeper craters and voids can be observed in Fig. 7a but a poor surface finish is found in Fig. 7b because of excess melting which leads to depletion of zinc from the parent material.

The micrographs for the Current 5 A, voltage 60 V and Pulse on Time 20 µs machining condition are shown in Fig. 8a and 8b at this condition small globules joined together to form a re-melted zone with small pits and voids results in average surface quality.

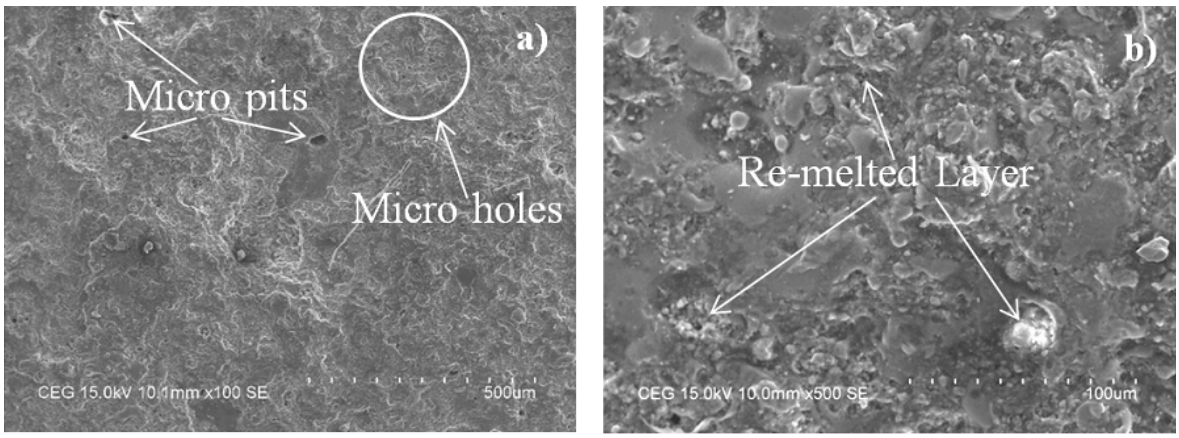

Fig. 6. SEM images for the optimal machining condition (I_p = 15 A, V_g = 55 V and T_{on} = 30 µs) a) lower magnification b) higher magnification

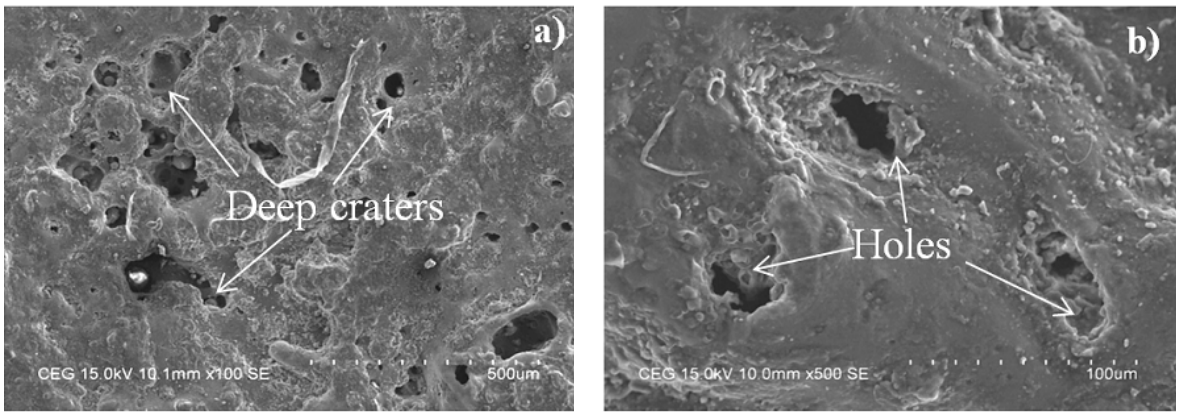

Fig. 7. SEM images for the machining condition of I_p = 15 A, V_g = 55 V and T_{on} = 10 µs a) lower magnification b) higher magnification

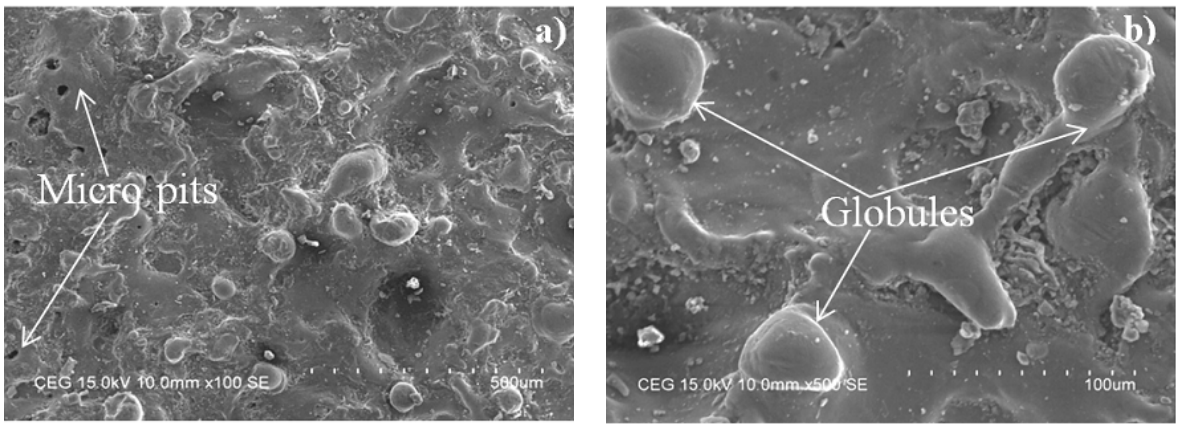

Fig. 8. SEM images for the machining condition of I_p = 5A, V_g = 60 V and T_{on} = 10 µs a) lower magnification b) higher magnification

4. Conclusions

The electrical discharge machining of AZ91 Magnesium alloy is successfully carried out using the Cu-TiB_2 tool. The input process parameters of current, voltage and pulse on time are considered and the output responses of MRR, TWR, and SR are observed. In order to attain the maximum MRR and minimum TWR & SR, the GRA and TOPSIS are employed and both the optimization techniques have given the optimal process parameters of I_p = 15 A, V_g = 55 V and T_{on} = 30 µs. The ANOVA is *performed* to investigate the influence of individual machining process parameters on the process characteristics. The pulse on time is the most influenced parameter followed by current and voltage. The SEM analysis shows that the initial machining condition creates more cracks, pits, holes and non-uniform surfaces. In optimal machining condition, the surface topography is better and showing fewer cracks and defects.

REFERENCES

[1] U. Riaz, I. Shabib, W. Haider, J. Biomed. Mater. Res. Part B. **107** (6), 1970-1996 (2019). DOI: https://doi.org/10.1002/jbm.b.34290

[2] M.K. Kulekci, Int. J. Adv. Manuf. Technol. **39** (9-10), 851-865 (2008). DOI: https://doi.org/10.1007/s00170-007-1279-2

[3] H. Furuya, N. Kogiso, S. Matunaga, K. Senda, Mater. Sci. Forum. **350**, 341-348 (2000). DOI: https://doi.org/10.4028/www.scientific.net/MSF.350-351.341

[4] S.N. Mathaudhu, E.A. Nyberg, Magnesium Alloys in U.S. Military Applications: Past, Current and Future Solutions. In: S.N. Mathaudhu, A.A. Luo, N.R. Neelameggham, E.A. Nyberg, W.H. Sillekens (eds) Essential Readings in Magnesium Technology. Springer, Cham (2016). DOI: https://doi.org/10.1007/978-3-319-48099-2_10

[5] V.V. Ramalingam, P. Ramasamy, M. Das Kovukkal, G. Myilsamy, Met. Mater. Int. **26** (4), 409-430 (2020). DOI: https://doi.org/10.1007/s12540-019-00346-8

[6] K.H. Ho, S.T. Newman, Int. J. Mach. Tools Manuf. **43** (13), 1287-1300 (2003). DOI: https://doi.org/10.1016/S0890-6955(03)00162-7

[7] M. Hourmand, A.A.D. Sarhan, M. Sayuti, Int. J. Adv. Manuf. Technol. **91** (1-4), 1023-1056, (2017). DOI: https://doi.org/10.1007/s00170-016-9671-4

[8] B. Nahak, A. Gupta, Manuf. Rev. **6** (2), 2019. DOI: https://doi.org/10.1051/mfreview/2018015

[9] S.S. Sidhu, A. Batish, S. Kumar, J. Reinf. Plast. Compos. **32** (17), 1310-1320 (2013). DOI: https://doi.org/10.1177/0731684413489366

[10] L. Arunkumar, B.K. Raghunath, Int. J. Eng. Technol. **5** (5), 4332-4338 (2013).

[11] Sohil Parsana, Nishil Radadia, Mohak Sheth, Nisarg Sheth, Vimal Savsani, N. Eswara Prasad, T. Ramprabhu, Arch. Civ. Mech. Eng. **18** (3), 799-817 (2018). DOI: https://doi.org/10.1016/j.acme.2017.12.007

[12] S. Santosh, S. Javed Syed Ibrahim, P. Saravanamuthukumar, K. Rajkumar, K.L. Hari Krishna, Appl. Mech. Mater. **787**, 406-410 (2015). DOI: https://doi.org/10.4028/www.scientific.net/AMM.787.406

[13] M. Hourmand, A.A.D. Sarhan, S. Farahany, M. Sayuti, Int. J. Adv. Manuf. Technol. **101** (9-12), 2723-2737 (2019). DOI: https://doi.org/10.1007/s00170-018-3130-3

[14] R. Ranjith, P. Tamilselvam, T. Prakash, C. Chinnasamy, Mater. Manuf. Process. **34** (10), 1120-1128 (2019). DOI: https://doi.org/10.1080/10426914.2019.1628258

[15] S. Tripathy, D.K. Tripathy, Mach. Sci. Technol. **21** (3), 362-384 (2017). DOI: https://doi.org/10.1080/10910344.2017.1283957

[16] S. Suresh Kumar, M. Uthayakumar, S. Thirumalai Kumaran, P. Parameswaran, E. Mohandas, G. Kempulraj, B.S. Ramesh Babu, S.A. Natarajan, J. Manuf. Process. **20**, 33-39 (2015). DOI: https://doi.org/10.1016/j.jmapro.2015.09.011

[17] P. Senthil, S. Vinodh, A.K. Singh, Int. J. Mach. Mach. Mater. **16** (1) 80-94 (2014). DOI: https://doi.org/10.1504/IJMMM.2014.063922

[18] K. Shunmugesh, K. Panneerselvam, Arch. Metall. Mater. **62** (3), 1803-1812 (2017). DOI: https://doi.org/10.1515/amm-2017-0273

[19] S.K. Ramuvel, S. Paramasivam, J. Mater. Res. Technol. **9** (3), 3885-3896 (2020). DOI: https://doi.org/10.1016/j.jmrt.2020.02.015

[20] A.K. Sahu, S.S. Mahapatra, S. Chatterjee, J. Thomas, Mater. Today:. Proc. **5** (9), 19019-19026 (2018). DOI: https://doi.org/10.1016/j.matpr.2018.06.253

[21] M. Eswara Krishna, P.K. Patowari, Mater. Manuf. Processes. **29** (9), 1131-1138 (2014). DOI: https://doi.org/10.1080/10426914.2014.930887

[22] A.S. Gill, S. Kumar, Arabian J. Sci. Eng. **43** (3), 1499-1510 (2017). DOI: https://doi.org/10.1007/s13369-017-2960-x

[23] P.K Rout, B. Surekha, P.C. Jena, G.N. Arko, Mater. Today: Proc. **26** (2), 2379-2387 (2020). DOI: https://doi.org/10.1016/j.matpr.2020.02.510

[24] M. Gostimirovic, P. Kovac, M. Sekulic, B. Skoric, J. Mech. Sci. Technol. **26** (1), 173-179 (2012). DOI: https://doi.org/10.1007/s12206-011-0922-x

[25] M. Ghoreishi, C. Tabari, Mater. Manuf. Processes, **22** (7-8), 833-841 (2007). DOI: https://doi.org/10.1080/10426910701446812

[26] M. Kiyak, B.E. Aldemir, E. Altan, Int. J. Adv. Manuf. Technol. **79** (1-4), 513-518 (2015). DOI: https://doi.org/10.1007/s00170-015-6840-9

[27] B.M. Schumacher, J. Mater. Process. Technol. **149** (1-3), 376-381 (2004). DOI: https://doi.org/10.1016/j.jmatprotec.2003.11.060

[28] L. Srinivasan, K. Mohammad Chand, T. Deepan Bharathi Kannan, P. Sathiya, S. Biju, Trans. Indian Inst. Met. **71** (2), 373-382 (2018). DOI: https://doi.org/10.1007/s12666-017-1166-y

[29] S. Tripathy, D.K. Tripathy, Eng. Sci. Technol. Int. J. **19** (1), 62-70 (2016). DOI: https://doi.org/10.1016/j.jestch.2015.07.010